PROCEEDINGS OF SCIENCE

Searches for invisible neutrino decay with KM3NeT/ORCA6

V. Carretero[a,*] **on behalf of the KM3NeT Collaboration**

[a] *IFIC (UV-CSIC),*
Carrer del Catedràtic José Beltrán Martinez, 2, 46980, Valencia, Spain

E-mail: vcarretero@km3net.de

In the era of precision measurements of the neutrino oscillation parameters, upcoming neutrino experiments will also be sensitive to physics beyond the Standard Model. ORCA is an atmospheric neutrino detector currently being built at the bottom of the Mediterranean Sea, that will measure atmospheric neutrino oscillation parameters with high precision and probe new physics at GeV energies. The final ORCA configuration of 115 string-like vertical detection units will be able to probe several theories beyond the Standard Model in neutrino physics. In this work, a three-flavour neutrino oscillation scenario in which the third neutrino mass state, ν_3, decays into an undetectable state, e.g., a sterile neutrino, is investigated with the first configuration of ORCA with six detection lines, ORCA6. A refined high-purity neutrino sample corresponding to 433 kton-years of data taking has been analysed and optimised for the search of this phenomenon. This contribution presents the bounds obtained in the decay parameter, $\alpha_3 = m_3/\tau_3$, and future sensitivity perspectives with ten years of data taking with the future ORCA configuration of 115 detection units.

38th International Cosmic Ray Conference (ICRC2023)
26 July - 3 August, 2023
Nagoya, Japan

*Speaker

PoS(ICRC2023)997

1. Introduction

KM3NeT is an ongoing research infrastructure situated on two sites of the Mediterranean Sea's seabed [1]. ARCA (Astroparticle Research with Cosmic in the Abyss) is positioned 100 km off the Sicilian coast near Capo Passero, Italy, at a depth of 3500 m. With a planned instrumented mass of 1 Gton of seawater, it is dedicated to the search for high-energy neutrinos from astrophysical sources. ORCA (Oscillation Research with Cosmic in the Abyss) is situated near Toulon, France, 40 km offshore at a depth of 2500 m and will cover approximately 7 Mton of seawater. ORCA aims to investigate neutrino oscillations and determine the neutrino mass ordering (NMO) by detecting neutrinos produced in the Earth's atmosphere [2].

The detection system consists of an array of pressure-resistant glass spheres denominated Digital Optical Modules (DOMs) housing 31 photomultiplier tubes (PMTs) and the corresponding readout boards [3]. The DOMs are supported by verticle flexible strings known as Detection Units (DUs), which are firmly anchored to the seabed. ORCA will have a total of 115 DUs, each containing 18 DOMs, vertically spaced by 9 m, while the horizontal separation between DUs is 20 m. Presently, 18 DUs have been deployed. The results presented herein correspond to the initial data collection using the 6-DU configuration referred to as ORCA6.

The detection principle employed by the ORCA detector relies on the Cherenkov effect, which occurs when charged particles surpass the speed of light in the medium and emit Cherenkov radiation. This detection mechanism allows for the accurate reconstruction of essential interaction parameters such as the interaction vertex, energy, direction, and event topology of the interacting neutrino. The resulting event topology exhibits specific characteristics, with track-like patterns for GeV muons produced in ν_μ-CC interactions and shower-like patterns for other neutrino channels.

The ORCA detector, currently under construction, has been continuously collecting data in the deep sea since mid-2019. From January 2020 to November 2021, data acquisition was carried out using the 6-DU configuration. A careful run selection process was implemented to ensure stringent data quality standards. Following this selection, a total of 510 days of high-quality data were included in the analysis, which, taking into account the current instrumented volume corrected by the working PMTs, corresponds to an exposure of 433 kton-years. Notably, a preliminary analysis searching for invisible neutrino decay was previously conducted using a subset of this dataset, comprising a total of 296 kton-years [4]. Several enhancements have been implemented in both the selection process and the subsequent analysis. Anti-noise cuts and a Boosted Decision Tree (BDT) machine learning algorithm are used to remove the atmospheric muon background (based on an atmospheric (atm.) muon score) and to discriminate between the two possible event topologies: track-like events and shower-like events, based on a track score.

After applying the pre-selection and removing events with high atm. muon scores, the remaining events are divided into two classes: tracks and showers. The track class is then subdivided into two subclasses based on the muon score, distinguishing well-reconstructed tracks from potentially misidentified atmospheric muons. This results in three distinct classes: High Purity Tracks, Low Purity Tracks, and Showers.

To further enhance the event selection, an additional criterion is implemented by imposing distinct thresholds for the reconstructed energy in the shower and track classes. Showers with a reconstructed energy exceeding 1 TeV and tracks with reconstructed energy above 100 GeV are

excluded. This specific threshold is chosen to mitigate the influence of unaccounted migrations from higher energies (above 10 TeV) in the simulation. Following this selection, it is expected that 5830 events will satisfy the criteria, whereas a total of 5828 events were observed in the dataset.

2. Invisible neutrino decay

Neutrino decay can be mathematically represented by a depletion factor, given by $D = e^{-\frac{t}{\tau_i}}$, where τ_i corresponds to the rest-frame lifetime of the mass state m_i, and t represents the proper time [5]. For relativistic neutrinos in the laboratory frame, the depletion factor can be expressed as $D = e^{-\frac{m_i L}{\tau_i E}}$, where L denotes the distance travelled by the neutrino and E represents its energy. This equation quantifies the fraction of neutrinos with a specific energy that remains intact after traversing a given distance. All three neutrino mass states can decay in principle, but in this analysis we focus on the third neutrino mass state, of which the invisible decay is not constrained from solar and supernova data, as it happens for ν_1 and ν_2. In order to allow for the invisible neutrino decay, a new term must be included in the Hamiltonian:

$$H_{\text{Total}} = \frac{1}{2E}\left[U\begin{pmatrix}0 & 0 & 0\\ 0 & \Delta m^2_{21} & 0\\ 0 & 0 & \Delta m^2_{31}\end{pmatrix}U^\dagger + U\begin{pmatrix}0 & 0 & 0\\ 0 & 0 & 0\\ 0 & 0 & -i\alpha_3\end{pmatrix}U^\dagger\right] + \begin{pmatrix}V & 0 & 0\\ 0 & 0 & 0\\ 0 & 0 & 0\end{pmatrix}, \tag{1}$$

where E is the neutrino energy, U is the Pontecorvo-Maki-Nakagawa-Sakata (PMNS) neutrino mixing matrix, $V = \pm\sqrt{2}N_e G_F$ being the matter potential, N_e, the electron density in matter and G_F, the Fermi constant. Essentially, the only change in the Hamiltonian is a shift in the mass basis term, from Δm^2_{31} to $\Delta m^2_{31} - i\alpha_3$.

As a consequence of neutrino decay, the mixing matrix becomes non-hermitian. Consequently, the total sum of neutrino oscillation probabilities deviates from unity,

$$P_{\beta e} + P_{\beta\mu} + P_{\beta\tau} = 1 - P_D(\beta) \qquad \beta = e, \mu, \tau, \tag{2}$$

where $P_D(\beta)$ is the decay probability for flavour β.

The impact of neutrino decay on the oscillation pattern can be observed in figure 1, depicting the decay effects on the survival (resp. transition) probability of muon (resp. electron) neutrinos. The oscillation parameter values used are obtained from NuFit 5.0 [8]. Notably, the decay effects induced by α_3 has a more pronounced impact on channels associated with the muon flavor, owing to the relatively higher contribution of ν_3 in the ν_μ component. Regardless of the mass ordering, the channel that experiences the most substantial effects of neutrino decay is $P_{\mu\mu}$.

The correlation between α_3 and θ_{23} exhibits a subtle yet distinct behavior in the oscillation and survival channels. Extensive investigations on the interplay between θ_{23} and α_3 have been conducted for specific baselines in references [6, 7]. However, in atmospheric neutrino experiments encompassing a wider range of baselines, this correlation becomes more complex. Figure 2 displays the muon neutrino survival probability (electron neutrino oscillation to muon) for four scenarios characterised by different $\theta_{23} - \alpha_3$ values. The decrease in the survival probability $P_{\mu\mu}$ at the oscillation maxima, induced by neutrino decay effects, can be partially compensated by reducing

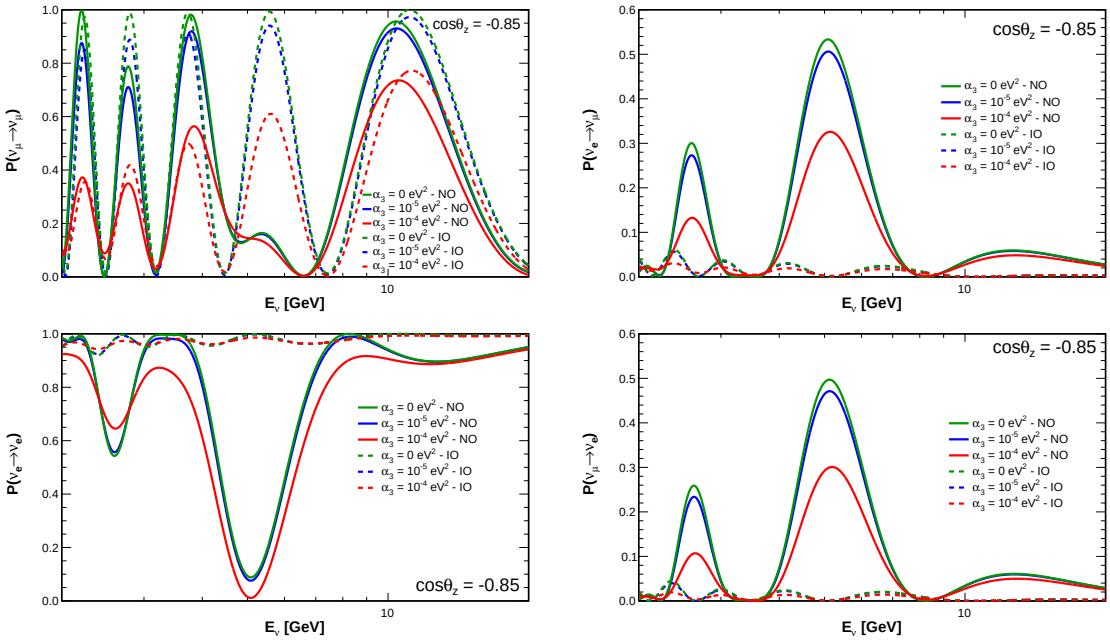

Figure 1: Probability for muon neutrino survival (top left), electron-to-muon transition (top right), electron neutrino survival (bottom left) and muon-to-electron transition (bottom right) as a function of energy at a cosine of the zenith angle $\cos\theta_z = -0.85$. Three values of the decay constant are considered: $\alpha_3 = 0$ (green), $\alpha_3 = 10^{-5}$ eV^2 (blue) and $\alpha_3 = 10^{-4}$ eV^2 (red). The solid (dashed) curves are for normal ordering, NO (inverted ordering, IO). Antineutrino probabilities can be described by the same curves but swapping the orderings.

the value of θ_{23} to the lower octant. However, such compensation results in an increased probability in the energy range where matter effects play a significant role. On the other hand, for the transition probability $P_{e\mu}$, a higher value of θ_{23} serves as a counterbalance to the decay-induced decrease. This will partially affect to the possibility to constrain both parameters at the same time.

3. Analysis

The analysis relies on 2-dimensional distributions of the reconstructed energy and reconstructed cosine of the zenith angle for each of the three event classes. These distributions are obtained through Swim [9], an analysis framework developed for KM3NeT which incorporates Monte Carlo (MC) simulations to model the detector response. Cross sections, neutrino fluxes, the interaction volume, and oscillation probabilities are taken into account when calculating the true energy and zenith angle distributions for each type of (anti)neutrino interaction.

Neutrinos are simulated from all angles and over a broad true energy range, from 1 GeV to 10 TeV. For the analysis, 10 bins in the reconstructed cosine of the zenith angle are used, and only reconstructed upward directions are taken into account. The reconstructed energies range from 2 to 1000 GeV, employing 15 unevenly spaced bins to ensure that each bin had enough statistics. Note that tracks with reconstructed energies above 100 GeV are rejected, so the 15th bin, which ranges from 100 to 1000 GeV, only contains shower events.

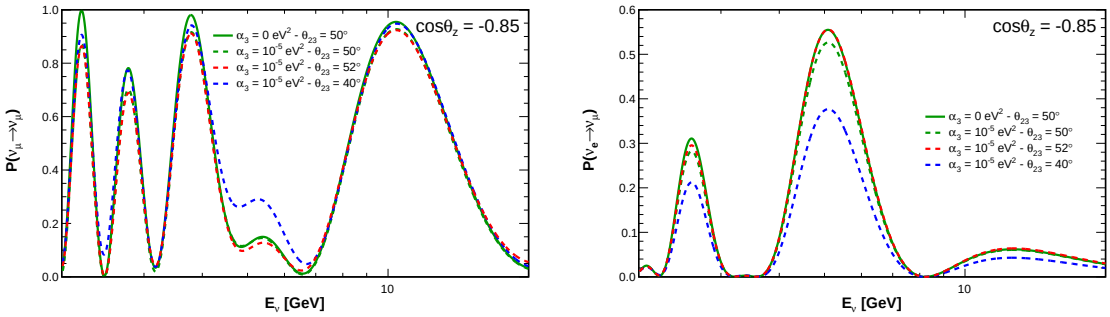

Figure 2: Probability for muon neutrino survival (left) and electron-to-muon transition (right) as a function of energy at a cosine of the zenith angle $\cos\theta_z = -0.85$ assuming NO. Four cases are shown: $\alpha_3 = 0$ with $\theta_{23} = 50°$ (solid green), $\alpha_3 = 10^{-5}$ eV^2 with the same value of θ_{23} (dashed green) and with two different values: $\theta_{23} = 52°$ (dashed red) and $\theta_{23} = 40°$ (dashed blue).

A response matrix is used to account for the detector resolution and it is evaluated by reconstructing MC events that relates true and reconstructed variables. For each interaction channel ν_x and class i, a 4-dimensional response matrix $R^{[\nu_x \to i]}(E_{\text{true}}, \theta_{\text{true}}, E_{\text{reco}}, \theta_{\text{reco}})$ is defined. Each entry within the matrix represents the efficiency of detection, classification, and reconstruction probability for a specific true bin $(E_{\text{true}}, \theta_{\text{true}})$. The expected interacting events are multiplied by these corresponding efficiencies to yield the reconstructed events of a given class i.

$$n^i_{\text{reco}}(E_{\text{reco}}, \theta_{\text{reco}}) = \sum_x n^x_{\text{int}}(E_{\text{true}}, \theta_{\text{true}}) \times R^{[\nu_x \to i]}(E_{\text{true}}, \theta_{\text{true}}, E_{\text{reco}}, \theta_{\text{reco}}), \tag{3}$$

The analysis method used to constrain the invisible decay parameter, α_3, is based on the maximization of a binned log-likelihood of the 2-dimensional distribution of events in $\log_{10}(E_{\text{reco}}/\text{GeV})$ and $\cos\theta_{\text{reco}}$, which compares the observed data to a model prediction. The sensitivities are computed using the Asimov approach, where the observed data is replaced by a representative dataset defined as the one which provides the expected values of the null hypothesis in each bin [10]. This analysis is not sensitive to θ_{13}, θ_{12}, Δm^2_{21} and δ_{CP}, so they are fixed to the NuFit 5.0 [8] values. Poisson distributions for the expected number of events in each bin and Gaussian distributions related to the nuisance parameters are used to model the log-likelihood:

$$-2\log L(\vec{\theta}) = \min_{\vec{\epsilon}} \left\{ 2 \sum_{i,j} \left[(N^{\text{mod}}_{ij}(\vec{\theta};\vec{\epsilon}) - N^{\text{dat}}_{ij}) + N^{\text{dat}}_{ij} \log\left(\frac{N^{\text{dat}}_{ij}}{N^{\text{mod}}_{ij}(\vec{\theta};\vec{\epsilon})} \right) \right] + \right. \tag{4}$$
$$\left. + \sum_k \left(\frac{\epsilon_k - \langle \epsilon_k \rangle}{\sigma_k} \right)^2 \right\}.$$

N^{mod}_{ij} and N^{dat}_{ij} represent the number of reconstructed events expected by the model and the number of events observed, respectively, in the bin (i,j). The parameter of interest, $\vec{\theta}$, is α_3 in this analysis. The parameters of the model that characterise the distributions $(\vec{\epsilon})$ are composed by nuisance parameters which are related to systematic uncertainties. Some of these parameters are constrained with priors representing constraints from other experiments. Specifically:

1. Normalisations: the overall normalisation as well as the relative normalisations of the High Purity Track and Shower classes are allowed to vary with no constraints. A 20% prior uncertainty is applied to the normalisation of neutral current (NC) and τ-CC events. At high energies (above 500 GeV), as a result of further approximations in the light propagation simulation in KM3NeT/ORCA, a 50% relative normalisation uncertainty is applied to events simulated in this regime.
2. Flux: the spectral index of the neutrino flux energy distribution, as $\phi \times E^s$, is allowed to vary from $s = 0$ with a standard deviation of 0.3. The ratio of electron neutrinos to electron antineutrinos is allowed to vary with a 7% prior uncertainty. The ratio of muon neutrinos to muon antineutrinos is allowed to vary with a 5% prior uncertainty. The ratio of muon neutrinos to electron neutrinos is allowed to vary with a 2% prior uncertainty. The ratio of vertical to horizontal neutrinos, introduced as $1 + r_{\mathrm{h/v}} \cos\theta$, is allowed to vary from $r_{\mathrm{h/v}} = 0$ with a standard deviation of 0.02.
3. The absolute energy scale of the detector is allowed to vary with a 9% prior uncertainty. The energy scale is related to the uncertainty on water optical properties and on the knowledge of the PMT efficiencies.
4. Oscillation parameters: Δm^2_{31} and θ_{23} are allowed to vary without constrains.

4. Results

The ORCA6 dataset has been studied to constrain the invisible decay parameter, α_3. The model is fitted to the dataset using 2-dimensional histograms on the reconstructed energy and direction. The results of the fit are subsequently transformed to the L/E (path length over neutrino energy) variable for the purpose of visualising the outcomes in figure 3. This is done for the standard case (stable scenario), decay (α_3 is freely fitted) and a high decay scenario to illustrate its effects ($\alpha_3 = 1.1 \times 10^{-3}\mathrm{eV}^2$, nuisance parameters are fixed to the decay best-fit).

The best-fit values for the parameters are $\sin^2\theta_{23} = 0.51^{+0.06}_{-0.07}$ and $\Delta m^2_{31} = 2.14^{+0.36}_{-0.25} \cdot 10^{-3}\mathrm{eV}^2$ for the standard case and $\sin^2\theta_{23} = 0.52^{+0.07}_{-0.07}$, $\Delta m^2_{31} = 2.21^{+0.33}_{-0.24} \cdot 10^{-3}\mathrm{eV}^2$ and $\alpha_3 = 1.08^{+1.4}_{-0.7} \cdot 10^{-4}\mathrm{eV}^2$ for the decay best-fit. The significance of the data preference to invisible neutrino decay compared to the stable scenario is estimated at 1.8σ.

The invisible neutrino decay parameter has been scanned and profiled in terms of the negative log-likelihood to provide a 1-dimensional scan in figure 4 (left) in comparison with the results of other experiments (T2K+NOνA combination [12], T2K+MINOS combination [13] and SK+K2K+MINOS combination [14]). The 2-dimensional scan to constrain θ_{23} and α_3 at the same time is shown as a 90% CL contour in figure 4 (right) compared to the previous ORCA6 result [4]. At every point in the contour, the log-likelihood is minimised relative to all nuisance parameters and the 90% CL contour is drawn through the recovered likelihood landscape.

Figure 5 shows the impact of the different systematic uncertainties is computed comparing the nominal best-fit value of α_3 with the result of the fit when fixing the considered nuisance parameter shifted $\pm$ its post-fit uncertainty. Black dots with error bars represent the pulls of the best-fit parameters. The error bars are computed as the post-fit uncertainty divided by the pre-fit uncertainty (priors). If the parameter was unconstrained, the pull is computed based on the post-fit uncertainty

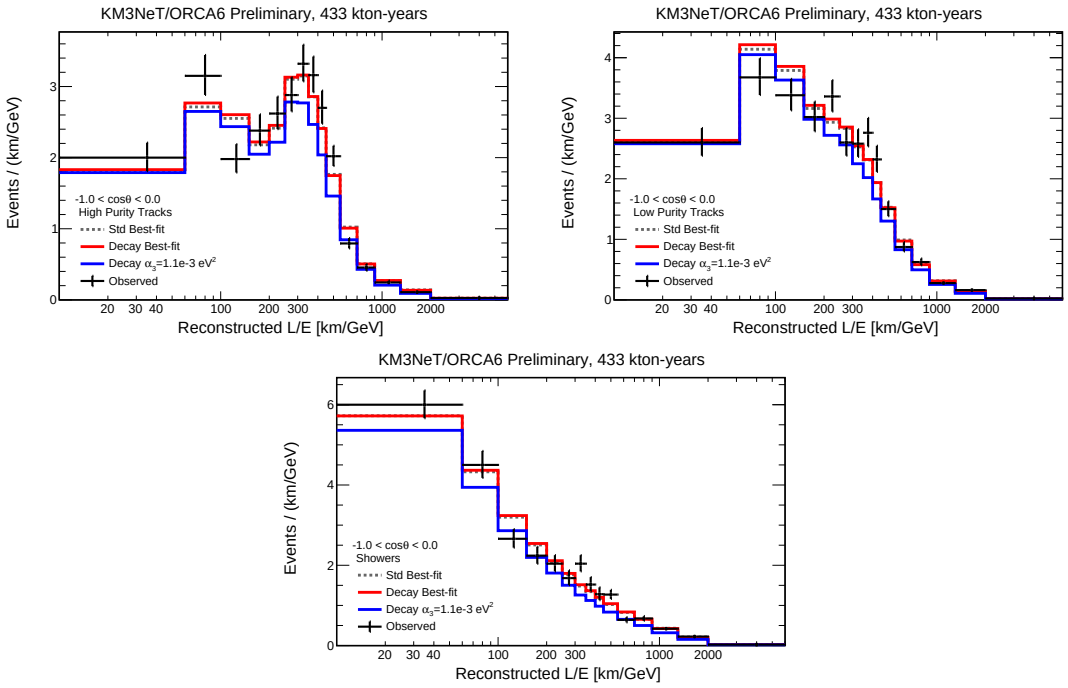

Figure 3: Distributions of the events divided by the bin width as a function of the reconstructed path length over neutrino energy, L/E, for the Standard bestfit (gray), decay bestfit (red), high decay scenario (blue) and data (black) for the three classes, High Purity Tracks (top left), Low Purity Tracks (top right) and Showers (bottom).

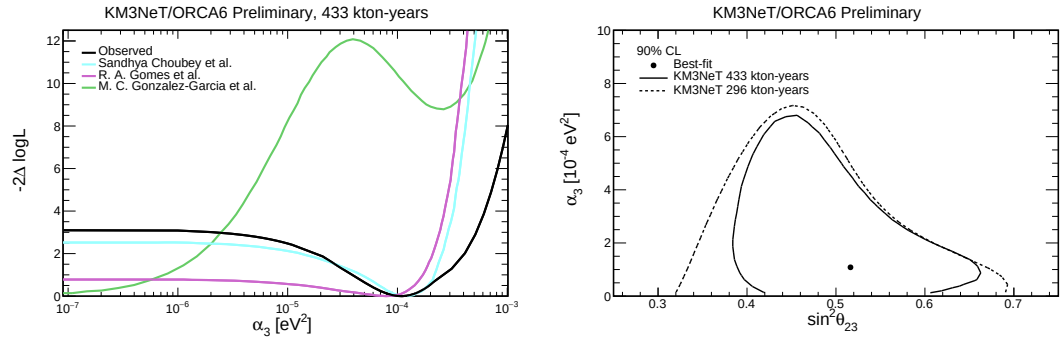

Figure 4: Profiled negative log-likelihood scan of the invisible neutrino decay parameter, α_3 (left) and 90% CL $\theta_{23} - \alpha_3$ contour (right).

and the error bar is 1. This test provides insights into the parameter correlations. Specifically, α_3 exhibits strong correlations with the normalisations, the spectral index, the horizontal to vertical flux ratio and θ_{23}.

5. Conclusions

With only 5% of its final configuration, the ORCA detector is starting to provide competitive results probing physics beyond the Standard Model such as the invisible neutrino decay. The best fit

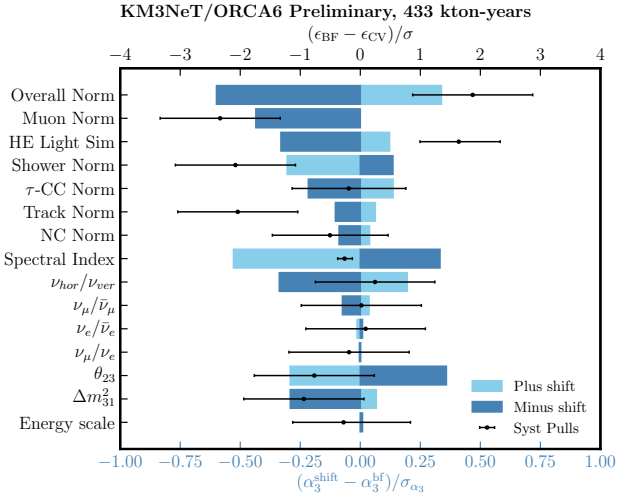

Figure 5: Impact of the different systematic parameters computed as a shift in the parameter of interest, α_3 when the nuisance parameter is shifted and fixed. Systematics Pulls are reported as black dots.

value is $\alpha_3 = 1.08^{+1.4}_{-0.7} \cdot 10^{-4}\text{eV}^2$ with a preference for invisible neutrino decay of 1.8σ with respect to the stable scenario. The detector deployment is progressing steadily and these measurements will improve as the detector volume gets larger and reconstruction and selection efficiencies are enhanced. Specifically, after 10 years of the complete ORCA115 detector, the 90% CL sensitivity is expected to improve by two orders of magnitude [15].

References

[1] KM3NeT Collaboration, DOI: 10.1088/0954-3899/43/8/084001
[2] KM3NeT Collaboration, DOI: 10.1140/epjc/s10052-021-09893-0
[3] KM3NeT Collaboration, DOI: 10.1088/1748-0221/17/07/P07038
[4] V. Carretero, DOI: 10.22323/1.414.0578
[5] G. Gelmini et al. DOI: 10.1016/0370-2693(84)91258-9
[6] S. Choubey et al. Doi: 10.1007/JHEP05(2021)133
[7] K. Chakraborty et al. DOI: 10.1007/JHEP05(2021)091
[8] I. Esteban et al, DOI: 10.1007/JHEP09(2020)178
[9] S. Bourret, https://theses.hal.science/tel-02491394
[10] G. Cowan et al. DOI: 10.1140/epjc/s10052-011-1554-0
[11] S.S. Wilks, DOI: 10.1214/aoms/1177732360
[12] Sandhya Choubey et al. DOI: 10.1007/JHEP08(2018)141
[13] R. A. Gomes et al. DOI: 10.1016/j.physletb.2014.12.014
[14] M. C. Gonzalez-Garcia et al. DOI: 10.1016/j.physletb.2008.04.041
[15] KM3NeT Collaboration. DOI: 10.1007/JHEP04(2023)090

PoS(ICRC2023)997

Full Authors List: The KM3NeT Collaboration

S. Aiello[a], A. Albert[b,bd], S. Alves Garre[c], Z. Aly[d], A. Ambrosone[f,e], F. Ameli[g], M. Andre[h], E. Androutsou[i], M. Anguita[j], L. Aphecetche[k], M. Ardid[l], S. Ardid[l], H. Atmani[m], J. Aublin[n], L. Bailly-Salins[o], Z. Bardačová[q,p], B. Baret[n], A. Bariego-Quintana[c], S. Basegmez du Pree[r], Y. Becherini[n], M. Bendahman[m,n], F. Benfenati[t,s], M. Benhassi[u,e], D. M. Benoit[v], E. Berbee[r], V. Bertin[d], S. Biagi[w], M. Boettcher[x], D. Bonanno[w], J. Boumaaza[m], M. Bouta[y], M. Bouwhuis[r], C. Bozza[z,e], R. M. Bozza[f,e], H.Brânzaş[aa], F. Bretaudeau[k], R. Bruijn[ab,r], J. Brunner[d], R. Bruno[a], E. Buis[ac,r], R. Buompane[u,e], J. Busto[d], B. Caiffi[ad], D. Calvo[c], S. Campion[g,ae], A. Capone[g,ae], F. Carenini[t,s], V. Carretero[c], T. Cartraud[n], P. Castaldi[af,s], V. Cecchini[c], S. Celli[g,ae], L. Cerisy[d], M. Chabab[ag], M. Chadolias[ah], A. Chen[ai], S. Cherubini[aj,w], T. Chiarusi[s], M. Circella[ak], R. Cocimano[w], J. A. B. Coelho[n], A. Coleiro[n], R. Coniglione[w] P. Coyle[d], A. Creusot[n], A. Cruz[al], G. Cuttone[w], R. Dallier[k], Y. Darras[ah], A. De Benedittis[e], B. De Martino[d], V. Decoene[k], R. Del Burgo[e], U. M. Di Cerbo[e], L. S. Di Mauro[w], I. Di Palma[g,ae], A. F. Díaz[j], C. Diaz[j], D. Diego-Tortosa[w], C. Distefano[w], A. Domi[ah], C. Donzaud[n], D. Dornic[d], M. Dörr[am], E. Drakopoulou[i], D. Drouhin[b,bd], R. Dvornický[q], T. Eberl[ah], E. Eckerová[q,p], A. Eddymaoui[m], T. van Eeden[r], M. Eff[n], D. van Eijk[r], I. El Bojaddaini[y], S. El Hedri[n], A. Enzenhöfer[d], G. Ferrara[w], M. D. Filipović[an], F. Filippini[t,s], D. Franciotti[w], L. A. Fusco[z,e], J. Gabriel[ao], S. Gagliardini[g], T. Gal[ah], J. García Méndez[l], A. Garcia Soto[c], C. Gatius Oliver[r], N. Geißelbrecht[ah], H. Ghaddari[y], L. Gialanella[e,u], B. K. Gibson[v], E. Giorgio[w], I. Goos[n], D. Goupilliere[o], S. R. Gozzini[c], R. Gracia[ah], K. Graf[ah], C. Guidi[ap,ad], B. Guillon[o], M. Gutiérrez[aq], H. van Haren[ar], A. Heijboer[r], A. Hekalo[am], L. Hennig[ah], J. J. Hernández-Rey[c], F. Huang[d], W. Idrissi Ibnsalih[e], G. Illuminati[s], C. W. James[al], M. de Jong[as,r], P. de Jong[ab,r], B. J. Jung[r], P. Kalaczyński[at,be], O. Kalekin[ah], U. F. Katz[ah], N. R. Khan Chowdhury[c], A. Khatun[q], G. Kistauri[av,au], C. Kopper[ah], A. Kouchner[aw,n], V. Kulikovskiy[ad], R. Kvatadze[av], M. Labalme[o], R. Lahmann[ah], G. Larosa[w], C. Lastoria[d], A. Lazo[c], S. Le Stum[d], G. Lehaut[o], E. Leonora[a], N. Lessing[c], G. Levi[t,s], M. Lindsey Clark[n], F. Longhitano[a], J. Majumdar[r], L. Malerba[ad], F. Mamedov[p], J. Mańczak[c], A. Manfreda[e], M. Marconi[ap,ad], A. Margiotta[t,s], A. Marinelli[e,f], C. Markou[i], L. Martin[k], J. A. Martínez-Mora[l], F. Marzaioli[u,e], M. Mastrodicasa[ae,g], S. Mastroianni[e], S. Miccichè[w], G. Miele[f,e], P. Migliozzi[e], E. Migneco[w], M. L. Mitsou[e], C. M. Mollo[e], L. Morales-Gallegos[u,e], C. Morley-Wong[al], A. Moussa[y], I. Mozun Mateo[ay,ax], R. Muller[r], M. R. Musone[e,u], M. Musumeci[w], L. Nauta[r], S. Navas[aq], A. Nayerhoda[ak], C. A. Nicolau[g], B. Nkosi[ai], B. Ó Fearraigh[ab,r], V. Oliviero[f,e], A. Orlando[w], E. Oukacha[n], D. Paesani[w], J. Palacios González[c], G. Papalashvili[au], V. Parisi[ap,ad], E.J. Pastor Gomez[c], A. M. Păun[aa], G. E. Păvălaş[aa], S. Peña Martínez[n], M. Perrin-Terrin[d], J. Perronnel[o], V. Pestel[ay], R. Pestes[n], P. Piattelli[w], C. Poirè[z,e], V. Popa[aa], T. Pradier[b], S. Pulvirenti[w], G. Quéméner[o], C. Quiroz[l], U. Rahaman[c], N. Randazzo[a], R. Randriatoamanana[k], S. Razzaque[az], I. C. Rea[e], D. Real[c], S. Reck[ah], G. Riccobene[w], J. Robinson[x], A. Romanov[ap,ad], A. Šaina[c], F. Salesa Greus[c], D. F. E. Samtleben[as,r], A. Sánchez Losa[c,ak], S. Sanfilippo[w], M. Sanguineti[ap,ad], C. Santonastaso[ba,e], D. Santonocito[w], P. Sapienza[w], J. Schnabel[ah], J. Schumann[ah], H. M. Schutte[x], J. Seneca[r], N. Sennan[y], B. Setter[ah], I. Sgura[ak], R. Shanidze[au], Y. Shitov[p], F. Šimkovic[q], A. Simonelli[e], A. Sinopoulou[a], M.V. Smirnov[ah], B. Spisso[e], M. Spurio[t,s], D. Stavropoulos[i], I. Štekl[p], M. Taiuti[ap,ad], Y. Tayalati[m], H. Tedjditi[ad], H. Thiersen[x], I. Tosta e Melo[a,aj], B. Trocmé[n], V. Tsourapis[i], E. Tzamariudaki[i], A. Vacheret[o], V. Valsecchi[w], V. Van Elewyck[aw,n], G. Vannoye[d], G. Vasileiadis[bb], F. Vazquez de Sola[r], C. Verilhac[n], A. Veutro[g,ae], S. Viola[w], D. Vivolo[u,e], J. Wilms[bc], E. de Wolf[ab,r], H. Yepes-Ramirez[l], G. Zarpapis[i], S. Zavatarelli[ad], A. Zegarelli[g,ae], D. Zito[w], J. D. Zornoza[c], J. Zúñiga[c], and N. Zywucka[x].

[a] INFN, Sezione di Catania, Via Santa Sofia 64, Catania, 95123 Italy

[b] Université de Strasbourg, CNRS, IPHC UMR 7178, F-67000 Strasbourg, France

[c] IFIC - Instituto de Física Corpuscular (CSIC - Universitat de València), c/Catedrático José Beltrán, 2, 46980 Paterna, Valencia, Spain

[d] Aix Marseille Univ, CNRS/IN2P3, CPPM, Marseille, France

[e] INFN, Sezione di Napoli, Complesso Universitario di Monte S. Angelo, Via Cintia ed. G, Napoli, 80126 Italy

[f] Università di Napoli "Federico II", Dip. Scienze Fisiche "E. Pancini", Complesso Universitario di Monte S. Angelo, Via Cintia ed. G, Napoli, 80126 Italy

[g] INFN, Sezione di Roma, Piazzale Aldo Moro 2, Roma, 00185 Italy

[h] Universitat Politècnica de Catalunya, Laboratori d'Aplicacions Bioacústiques, Centre Tecnològic de Vilanova i la Geltrú, Avda. Rambla Exposició, s/n, Vilanova i la Geltrú, 08800 Spain

[i] NCSR Demokritos, Institute of Nuclear and Particle Physics, Ag. Paraskevi Attikis, Athens, 15310 Greece

[j] University of Granada, Dept. of Computer Architecture and Technology/CITIC, 18071 Granada, Spain

[k] Subatech, IMT Atlantique, IN2P3-CNRS, Université de Nantes, 4 rue Alfred Kastler - La Chantrerie, Nantes, BP 20722 44307 France

[l] Universitat Politècnica de València, Instituto de Investigación para la Gestión Integrada de las Zonas Costeras, C/ Paranimf, 1, Gandia, 46730 Spain

[m] University Mohammed V in Rabat, Faculty of Sciences, 4 av. Ibn Battouta, B.P. 1014, R.P. 10000 Rabat, Morocco

[n] Université Paris Cité, CNRS, Astroparticule et Cosmologie, F-75013 Paris, France

[o] LPC CAEN, Normandie Univ, ENSICAEN, UNICAEN, CNRS/IN2P3, 6 boulevard Maréchal Juin, Caen, 14050 France

[p] Czech Technical University in Prague, Institute of Experimental and Applied Physics, Husova 240/5, Prague, 110 00 Czech Republic

[q] Comenius University in Bratislava, Department of Nuclear Physics and Biophysics, Mlynska dolina F1, Bratislava, 842 48 Slovak Republic

[r] Nikhef, National Institute for Subatomic Physics, PO Box 41882, Amsterdam, 1009 DB Netherlands

[s] INFN, Sezione di Bologna, v.le C. Berti-Pichat, 6/2, Bologna, 40127 Italy

[t] Università di Bologna, Dipartimento di Fisica e Astronomia, v.le C. Berti-Pichat, 6/2, Bologna, 40127 Italy

[u] Università degli Studi della Campania "Luigi Vanvitelli", Dipartimento di Matematica e Fisica, viale Lincoln 5, Caserta, 81100 Italy

[v] E. A. Milne Centre for Astrophysics, University of Hull, Hull, HU6 7RX, United Kingdom

[w] INFN, Laboratori Nazionali del Sud, Via S. Sofia 62, Catania, 95123 Italy
[x] North-West University, Centre for Space Research, Private Bag X6001, Potchefstroom, 2520 South Africa
[y] University Mohammed I, Faculty of Sciences, BV Mohammed VI, B.P. 717, R.P. 60000 Oujda, Morocco
[z] Università di Salerno e INFN Gruppo Collegato di Salerno, Dipartimento di Fisica, Via Giovanni Paolo II 132, Fisciano, 84084 Italy
[aa] ISS, Atomistilor 409, Măgurele, RO-077125 Romania
[ab] University of Amsterdam, Institute of Physics/IHEF, PO Box 94216, Amsterdam, 1090 GE Netherlands
[ac] TNO, Technical Sciences, PO Box 155, Delft, 2600 AD Netherlands
[ad] INFN, Sezione di Genova, Via Dodecaneso 33, Genova, 16146 Italy
[ae] Università La Sapienza, Dipartimento di Fisica, Piazzale Aldo Moro 2, Roma, 00185 Italy
[af] Università di Bologna, Dipartimento di Ingegneria dell'Energia Elettrica e dell'Informazione "Guglielmo Marconi", Via dell'Università 50, Cesena, 47521 Italia
[ag] Cadi Ayyad University, Physics Department, Faculty of Science Semlalia, Av. My Abdellah, P.O.B. 2390, Marrakech, 40000 Morocco
[ah] Friedrich-Alexander-Universität Erlangen-Nürnberg (FAU), Erlangen Centre for Astroparticle Physics, Nikolaus-Fiebiger-Straße 2, 91058 Erlangen, Germany
[ai] University of the Witwatersrand, School of Physics, Private Bag 3, Johannesburg, Wits 2050 South Africa
[aj] Università di Catania, Dipartimento di Fisica e Astronomia "Ettore Majorana", Via Santa Sofia 64, Catania, 95123 Italy
[ak] INFN, Sezione di Bari, via Orabona, 4, Bari, 70125 Italy
[al] International Centre for Radio Astronomy Research, Curtin University, Bentley, WA 6102, Australia
[am] University Würzburg, Emil-Fischer-Straße 31, Würzburg, 97074 Germany
[an] Western Sydney University, School of Computing, Engineering and Mathematics, Locked Bag 1797, Penrith, NSW 2751 Australia
[ao] IN2P3, LPC, Campus des Cézeaux 24, avenue des Landais BP 80026, Aubière Cedex, 63171 France
[ap] Università di Genova, Via Dodecaneso 33, Genova, 16146 Italy
[aq] University of Granada, Dpto. de Física Teórica y del Cosmos & C.A.F.P.E., 18071 Granada, Spain
[ar] NIOZ (Royal Netherlands Institute for Sea Research), PO Box 59, Den Burg, Texel, 1790 AB, the Netherlands
[as] Leiden University, Leiden Institute of Physics, PO Box 9504, Leiden, 2300 RA Netherlands
[at] National Centre for Nuclear Research, 02-093 Warsaw, Poland
[au] Tbilisi State University, Department of Physics, 3, Chavchavadze Ave., Tbilisi, 0179 Georgia
[av] The University of Georgia, Institute of Physics, Kostava str. 77, Tbilisi, 0171 Georgia
[aw] Institut Universitaire de France, 1 rue Descartes, Paris, 75005 France
[ax] IN2P3, 3, Rue Michel-Ange, Paris 16, 75794 France
[ay] LPC, Campus des Cézeaux 24, avenue des Landais BP 80026, Aubière Cedex, 63171 France
[az] University of Johannesburg, Department Physics, PO Box 524, Auckland Park, 2006 South Africa
[ba] Università degli Studi della Campania "Luigi Vanvitelli", CAPACITY, Laboratorio CIRCE - Dip. Di Matematica e Fisica - Viale Carlo III di Borbone 153, San Nicola La Strada, 81020 Italy
[bb] Laboratoire Univers et Particules de Montpellier, Place Eugène Bataillon - CC 72, Montpellier Cédex 05, 34095 France
[bc] Friedrich-Alexander-Universität Erlangen-Nürnberg (FAU), Remeis Sternwarte, Sternwartstraße 7, 96049 Bamberg, Germany
[bd] Université de Haute Alsace, rue des Frères Lumière, 68093 Mulhouse Cedex, France
[be] AstroCeNT, Nicolaus Copernicus Astronomical Center, Polish Academy of Sciences, Rektorska 4, Warsaw, 00-614 Poland

Acknowledgements

The authors acknowledge the financial support of the funding agencies: Agence Nationale de la Recherche (contract ANR-15-CE31-0020), Centre National de la Recherche Scientifique (CNRS), Commission Européenne (FEDER fund and Marie Curie Program), LabEx UnivEarthS (ANR-10-LABX-0023 and ANR-18-IDEX-0001), Paris Île-de-France Region, France; Shota Rustaveli National Science Foundation of Georgia (SRNSFG, FR-22-13708), Georgia; The General Secretariat of Research and Innovation (GSRI), Greece Istituto Nazionale di Fisica Nucleare (INFN), Ministero dell'Università e della Ricerca (MIUR), PRIN 2017 program (Grant NAT-NET 2017W4HA7S) Italy; Ministry of Higher Education, Scientific Research and Innovation, Morocco, and the Arab Fund for Economic and Social Development, Kuwait; Nederlandse organisatie voor Wetenschappelijk Onderzoek (NWO), the Netherlands; The National Science Centre, Poland (2021/41/N/ST2/01177); The grant "AstroCeNT: Particle Astrophysics Science and Technology Centre", carried out within the International Research Agendas programme of the Foundation for Polish Science financed by the European Union under the European Regional Development Fund; National Authority for Scientific Research (ANCS), Romania; Grants PID2021-124591NB-C41, -C42, -C43 funded by MCIN/AEI/ 10.13039/501100011033 and, as appropriate, by "ERDF A way of making Europe", by the "European Union" or by the "European Union NextGenerationEU/PRTR", Programa de Planes Complementarios I+D+I (refs. ASFAE/2022/023, ASFAE/2022/014), Programa Prometeo (PROMETEO/2020/019) and GenT (refs. CIDEGENT/2018/034, /2019/043, /2020/049. /2021/23) of the Generalitat Valenciana, Junta de Andalucía (ref. SOMM17/6104/UGR, P18-FR-5057), EU: MSC program (ref. 101025085), Programa María Zambrano (Spanish Ministry of Universities, funded by the European Union, NextGenerationEU), Spain; The European Union's Horizon 2020 Research and Innovation Programme (ChETEC-INFRA - Project no. 101008324).